IJFANS INTERNATIONAL JOURNAL OF FOOD AND NUTRITIONAL SCIENCES

ISSN PRINT 2319 1775 Online 2320 7876

 Journal Volume 10, Iss 09, 2021

SUPRAMOLECULAR ARCHITECTURE AND PHOTOPHYSICAL AND BIOLOGICAL PROPERTIES OF RUTHENIUM(II) POLYPYRIDYL COMPLEXES

[1]MAGGIDI RAMANI,[2]GOVARDHAN SREENANCHA,[3]SRIKANTH NYAMTABAD

[123]*Assistant Professor*

Department of Chemistry

Kshatriya College of Engineering

ABSTRACT:

Complexes of the type [Ru(N–N)2(tdzp)]Cl2, where N–N is 2,20 -bipyridine (bpy) (1), 1,10-phenathroline (phen) (2), dipyrido[3,2-d:20 ,3-f] quinoxaline (dpq) (3), which incorporate the [1,2,5]-thiadiazolo-[3,4-f]- [1,10]-phenanthroline (tdzp) ligand, have been synthesized and characterized by IR, 1 H-NMR, 13C-NMR, ESI-MS, elemental analysis, UV-Visible and luminescence spectroscopy. The molecular structure of complex 2 is confirmed by single crystal X-ray structure determination. A two-dimensional cyclic water– chloride anionic {[(H2O)10(Cl)2] 2}n network has been structurally identified in a hydrophobic matrix of 2. Interaction of these complexes with Calf Thymus DNA (CT-DNA) was explored by electronic absorption and emission spectroscopy and circular dichroism spectroscopy. The nucleolytic cleavage activity of complexes 1–3 has been carried out on double stranded circular plasmid pBR322 DNA by gel electrophoresis experiments. The cytotoxicity of the complexes against a cancer cell line has been studied by MTT assay and cellular localization of complexes within the cells has been monitored by fluorescence microscopy. Notably, 1–3 exhibit potent antiproliferative activities against a panel of human cancer cell line.

Introduction

Deoxyribonucleic acid (DNA) is the primary carrier of all genetic information and it plays a major role in replication and storage of genes. Thus the molecules that interact with DNA have a variety of applications including pharmaceuticals, tools for molecular biology and probes for electron transfer.1,2 In this context, over the last two decades the transition metal polypyridyl complexes have received a considerable amount of attention.3–12 In particular coordinatively saturated ruthenium(II) polypyridyl complexes have received much attention because of their tuneable photophysical and photochemical properties, leading to a wide range of successful or potential applications in the field of photochemistry, photo-physics, and biochemistry.4,5,13,14 A widely studied [Ru(bpy)3] 2+ (bpy = 2,20 -bipyridine) complex binds electrostatically to DNA having binding affinity in the order of 103 M1 , 15 but when one of the bpy ligands is replaced with a dppz (dppz = dipyrido[3,2-a:20 ,30 -c]phenazine) ligand, it results in the [Ru(bpy)2(dppz)]2+ complex that binds intercalatively to DNA with a binding constant of the order 106 M1 and this complex also behaves as a molecular light switch for DNA.2,16,17 This shows that the DNA interaction properties of complexes can be tuned by modification of ligands. Ruthenium polypyridyl complexes interact with DNA by non-covalent interaction such as electrostatic, minor groove, major groove, partial intercalative and intercalative binding modes.18 However, there is still uncertainty on the exact location of binding modes. Further studies are necessary using different structural ligands to evaluate and

ISSN PRINT 2319 1775 Online 2320 7876

 Journal Volume 10, Iss 09, 2021

understand the factors that determine the DNA binding modes.

It has been largely accepted that ruthenium(II) polypyridyl complexes can be used as probes for DNA structure determination,5,19,20,21 DNA photo-cleavage agents and DNA mediated electron transfer.13,22 Recent reports on advantages of ruthenium complexes as potential cellular imaging and anticancer agents has drawn much attention.4,5,20–36 In this context, recently Liang-Nian Ji and co-workers have reported the effect of hydrophobicity and the surface area of the ancillary ligands on the DNA binding and cytotoxicity properties of ruthenium complexes.31–34 More recently, J. Thomas and co-workers36 have reported the successful application of a dinuclear ruthenium(II) polypyridyl 'light switch' complex as an in cellulo nuclear stain, well tolerated by eukaryotic and prokaryotic cells. These results show that versatility of these complexes can be modified by the ligand set, which controls whether the complex is an intercalator, hemiintercalator or electrostatic binder.

As part of a project aimed at systematic structural alteration with a view to elucidating structure–activity relationships, here we report the synthesis, characterization, structural properties, DNA binding, DNA cleavage and preliminary anticancer activity of new complexes of the type [Ru(N–N)2(tdzp)]Cl2, where N–N is 2,20 -bipyridine (bpy) (1), 1,10-phenanthroline (phen) (2), dipyrido [3,2-d:20 ,3f] quinoxaline (dpq) (3), which incorporate [1,2,5]- thiadiazolo-[3,4-f]-[1,10]-phenanthroline (tdzp) (Scheme 1) as the ancillary ligand. Interestingly, complex 2 acts as a building block, generating a supramolecular framework encapsulating a cyclic hybrid chloride–water cluster {[(H2O)10(Cl)2] 2}n.

Results and discussions

Synthesis and characterization

[1,2,5]-Thiadiazolo-[3,4-f]-[1,10]-phenanthroline (tdzp) was synthesized as per literature procedure in four steps.37,38 The ruthenium(II) polypyridyl complexes of the type [Ru(N–N)2(tdzp)]2+ (1–3) (where, NN = bpy, phen, dpq) were synthesized by refluxing a 1 : 1 molar ratio of cis-[Ru(NN)2Cl2] and the [1,2,5]-thiadiazolo- [3,4-f]-[1,10]-phenanthroline (tdzp) ligand in methanol water mixture (1 : 1). The complexes obtained were purified by column chromatography using an activated neutral alumina column and obtained as racemic mixtures. The complexes were characterized by 1 H NMR, 13C NMR, IR, elemental analysis, UV-Visible spectroscopy and electrospray mass spectrometry (see the Experimental section). In ESI-MS peaks due to [M–Cl]+ and [M–2Cl]2+ were observed. The further physio-chemical and biological studies were carried out using the racemic mixtures.

Crystal structure of 210H2O. Crystals of complex 210H2O suitable for single crystal X-ray structure determination were grown by slow evaporation of solution of complex 2 in water :methanol

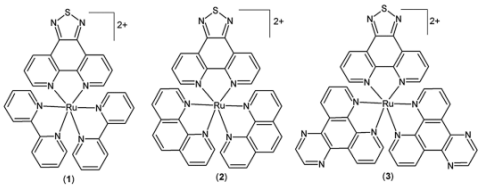

Scheme 1 Molecular structures of complexes 1–3.

ISSN PRINT 2319 1775 Online 2320 7876

 Journal Volume 10, Iss 09, 2021

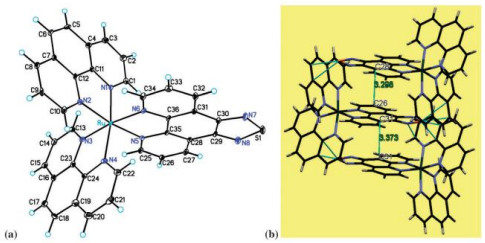

Fig. 1 (a) ORTEP diagram of the cation of 2, anions and solvent molecules were omitted for clarity, (b) pi–pi aromatic stacking interactions between planar tdzp ligands in 2. Selected bond lengths (Å): Ru–N1 = 2.060(5); Ru–N2 = 2.066(5); Ru–N3 = 2.054(5); Ru–N4 = 2.062(5); Ru–N5 = 2.053(5); Ru–N6 = 2.071(5). Selected bond angles (1): N(1)–Ru–N(2) = 79.80(2); N(3)–Ru–N(4) = 79.80(2); N(5)–Ru–N(6) = 79.95(2).

mixture at room temperature. An ORTEP diagram of cation of complex 2 is given in Fig. 1a. The complex crystallizes in the triclinic space group P1. Relevant crystallographic information % for complex 2 is given in Table S1 (ESI†), and a list of selected bond lengths and angles can be found in Table S2 (ESI†). The complex 2 crystallizes with ten water molecules and the two chloride anions were disordered over three positions. The ruthenium(II) was chelated by one tdzp ligand and two phenanthroline ligands. The coordination geometry around the ruthenium centre can be described as distorted octahedral, with an average bite angle of 79.85(2)1 between three polypyridyl ligands. The average Ru–N (1,10-phenatroline) bond length is 2.060(5) Å and Ru–N (tdzp) bond length is 2.061(5) Å, which is similar to the reported analogues mix ligand ruthenium(II) polypyridyl complexes.39–43 The crystal structure exhibits p–p aromatic stacking interactions involving a planar tdzp ligand with an inter-planar distance of 3.373 Å (C28–C26)/3.298 Å (C31–C31) (Fig. 1b).

Supramolecular architecture of 210H2O containing cyclic hybrid water–chloride cluster. Hydrated halide anions are an extremely active area of research, because they are the most common anions in nature due to their role in many chemical, environmental, and biological processes.44,45 Further studies on structures of halide–water clusters in nature is of fundamental importance for the understanding of the water–halide interaction in the atmosphere, ocean and biological systems.44,46,47 In particular, water–chloride interactions is one of the most commonly found interactions in nature (e.g., seawater or sea-salt aerosols), and thus the examination of water–chloride interactions has been the object of numerous theoretical studies.

Table 1 Selected hydrogen-bonding parameters[a]

D–H···A	D–H (Å)	H···A (Å)	D···A (Å)	D–H···A (°)
C1–H1···Cl2	0.95	2.67	3.431(7)	138.0
C9–H9···O3W^{i}	0.95	2.46	3.405(9)	170.8
C10–H10···O6W^{i}	0.95	2.45	3.236(9)	140.1
C21–H21···Cl2^{i}	0.95	2.87	3.815(7)	175.9
C25–H25···O1W^{ii}	0.95	2.55	3.326(10)	138.5
C26–H26···Cl3	0.95	2.73	3.676(7)	178.0
O1W–H1W1···Cl1	0.82(2)	2.33(3)	3.121(8)	164(10)
O1W–H1W2···S1^{iii}	0.82(2)	2.82(4)	3.620(9)	166(10)
O2W–H2W2···Cl3	0.83(2)	2.21(9)	2.876(12)	137(11)
O3W–H3W1···Cl1	0.82(2)	2.24(2)	3.056(7)	176(8)
O3W–H3W2···O7W^{iv}	0.81(2)	2.01(2)	2.815(8)	172(6)
O4W–H4W1···Cl1	0.84(2)	2.32(3)	3.147(8)	169(9)
O4W–H4W2···O2W^{v}	0.83(2)	2.03(4)	2.812(15)	157(8)
O5W–H5W1···O1W^{ii}	0.82(2)	2.14(2)	2.951(10)	174(7)
O5W–H5W2···O7W	0.81(2)	2.14(4)	2.863(8)	148(8)
O6W–H6W1···O3W	0.82(2)	2.03(2)	2.842(8)	173(6)
O6W–H6W2···O8W	0.81(2)	1.99(2)	2.803(9)	177(6)
O7W–H7W1···O9W	0.82(2)	2.00(5)	2.711(8)	144(8)
O7W–H7W2···O6W	0.82(2)	1.90(2)	2.718(8)	177(6)
O8W–H8W1···O4W	0.82(2)	2.08(7)	2.712(10)	134(9)
O8W–H8W2···O6W	0.81(2)	2.34(9)	2.803(9)	117(8)
O9W–H9W1···Cl1^{ii}	0.84(2)	2.33(7)	3.073(7)	147(11)
O9W–H9W2···O7W	0.83(2)	1.90(2)	2.711(8)	168(8)
O10W–H101···O8W	0.81(2)	2.01(5)	2.751(9)	153(9)
O10W–H102···Cl2	0.82(2)	2.27(3)	3.060(9)	164(9)

a Symmetry code(s): (i) x, y + 1, z; (ii) x + 1, y, z; (iii) x + 1, y + 1, z + 1; (iv) x + 1, y, z + 2; (v) x 1, y, z.

Recently several water chloride clusters in various crystal systems have been identified and structurally characterized.44,48,51 such as {[(H2O)20(Cl)4] 4}n, 48 [(H2O)6(Cl)2] 2, 51 [(H2O)10(Cl)2] 2. 44 These investigations are believed to provide an input towards the understanding of the

ISSN PRINT 2319 1775 Online 2320 7876

 Journal Volume 10, Iss 09, 2021

hydration phenomena of chloride anions in nature and have importance in supramolecular chemistry, catalysis, biochemistry.

Interestingly in the crystal structure of 2 extensive hydrogen bonding interactions are observed between the all lattice water molecules and chloride anions (Table 1) leading to the formation

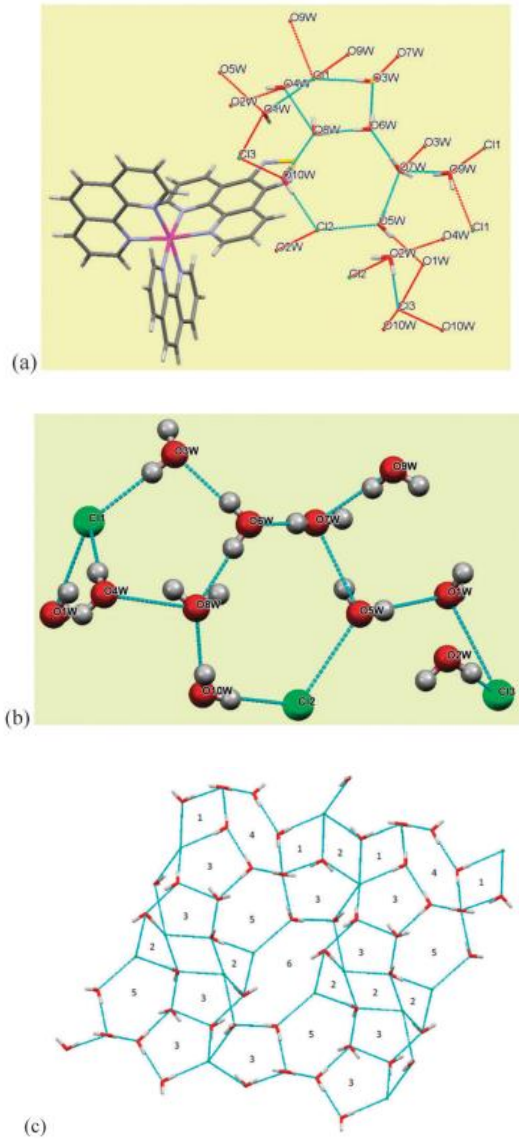

Fig. 2 (a) Ru(II) cationic building block 2 showing (arbitrary view) hydrogen bonding interactions between chloride anions and water molecules, (b) a closer view of the cyclic water–chloride cluster in 2, (c) nonplanar 2D anionic layer (arbitrary view) generated by the water–chloride cluster {[(H2O)10Cl2] 2}n.

of a polymeric hybrid cyclic water–chloride cluster possessing minimal repeating {[(H2O)10(Cl)2] 2}n units (Fig. 2). The arrangement of atoms in the cyclic water–chloride cluster along with a proper atom labelling scheme is shown in Fig. 2. Each cyclic cluster consists of two chloride and ten water molecules, is connected to the next cyclic unit by the tail, having one water molecule. These clusters further interconnected by hydrogen bonding leading to a non-polar 2D water–chloride anionic layer (Fig. 2c). A packing diagram of 2 shows the arrangement of cationic molecules with tdzp ligands face to face by p–p stacking with the formation of channels encapsulating 2D water–chloride clusters. The space fill model of crystal packing of 2 view down the ‘c’ axis (Fig. 3 and Fig. S7, ESI†) shows that a 2D anionic hybrid water–chloride cluster {[(H2O)10(Cl)2] 2}n occupies the free space between hydrophobic arrays of the metal–organic part, with an inter layer separation of 11.907 Å which is equal to the b unit cell dimension (Table S1, ESI†). Nevertheless seven weak C–HCl/C–HO/O–HS hydrogen bonds [average d(DA) = 3.501 (Å)] between a metal–organic unit and chloride– water molecules (Table 1) lead to the formation of a 3D supramolecular framework. The selected hydrogen bonding parameters are given in Table 1. The different chloride anions are strongly held in lattice by O–HCl and C–HCl hydrogen bonds (Fig. S7, ESI†), Cl1 is held between three nearby water molecules [O1–H1Cl1 = 3.121 Å, O3–H3Cl1 = 3.148 Å and O4–H4Cl2 = 3.056 Å]. Similar hydrogen bonding is also observed for Cl2 [O5–H5Cl2 = 3.066 Å and O10–H10Cl2 = 3.066 Å]. The ClO separations are smaller than those previously reported for Cl(H2O)4 52 and

ISSN PRINT 2319 1775 Online 2320 7876

 Journal Volume 10, Iss 09, 2021

Cl2(H2O) OO distances are in the range from 2.711 to 2.863 Å with an average value of 2.79 Å, which can be compared with OO distances of 2.76 Å in hexagonal (Ih) ice (at 200 K),55 2.74 Å in cubic (Ic) ice56 or 2.85 Å in liquid water.57 OOO angles vary from 102.25 to 124.271 with an average of 112.71 which slightly deviated from the angle of 109.31 on hexagonal ice.55 Seven of ten water molecules participative in the formation of three hydrogen bonds each (accepting one hydrogen and donating two), while the O2, O7, and O10 water molecules along with Cl1 and Cl2 are involved in four hydrogen bonding contacts. The different cyclic fragments in the 2D network (Fig. 2c) are classified in Table 2. Altogether there are six different cycles, that is two tetra-nuclear, one penta-nuclear, two hexa-nuclear and one-dodeca nuclear fragments (Fig. 2c and Table 2). One of them contains only water molecules, while other five rings are chloride–water hybrids with one or two or four chloride atoms. The lengthy OO or ClCl non-bonding separations within the fragments vary from 4.449 to 14.307 Å (Table 2).

Moreover, the present finding extends the still limited number48–51 of the well-characterized examples of large polymeric 2D water–chloride assemblies intercalated in crystalline materials and shows that [1,2,5]-thiadiazolo-[3,4-f]-[1,10]-phenanthroline (tdzp) complexes can offer rather appropriate matrixes to stabilize and store water–chloride clusters. Further work is currently under progress aiming to get more information about how the modification of the [1,2,5]-thiadiazolo-[3,4-f]-[1,10]- phenanthroline (tdzp) ligand or the replacement of chlorides by other counter ions with a high accepting capacity toward

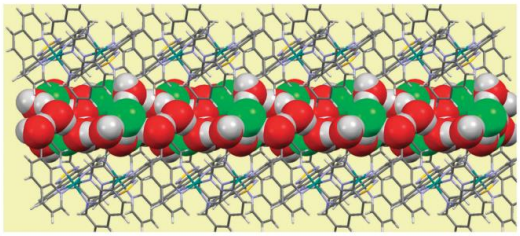

Fig. 3 Crystal packing diagram space fill model showing water–chlorine water channels along the ‘c’ axis.

Table 2 Description of cyclic fragments within the water–chloride network in 2

Cycle number	Number of O/Cl atoms	Formula	Atom numbering scheme	Geometry	Most lengthy non-bonding separation (Å)
1	4	$[(H_2O)_3(Cl)]^-$	O_1–O_3–O_4–Cl_1	Planar	$O_3\cdots Cl_1$, 4.449
2	4	$[(H_2O)_3(Cl)_1]^{2-}$	O_8–Cl_2–O_8–Cl_1	Planar/non-planar	$Cl_1\cdots Cl_1$, 4.707
3	5	$[(H_2O)_4(Cl)]^-$	O_5–O_6–O_9–O_7–Cl_1	Non-planar	$O_5\cdots O_9$, 4.712
4	6	$[(H_2O)_6]$	O_2–O_8–O_7–O_2–O_8–O_7	Planar	$O_7\cdots O_8$, 6.282
5	6	$[(H_2O)_5(Cl)]^-$	O_{10}–O_7–O_6–O_9–O_{10}–Cl_2	Non-planar	$O_7\cdots O_{10}$, 5.802
6	12	$[(H_2O)_8(Cl)_4]^{4-}$	O_3–O_5–Cl_2–O_3–O_9–Cl_1–O_5–O_3–Cl_2–O_7–O_9–Cl_1	Non-planar	$Cl_1\cdots Cl_1$, 14.309

hydrogen-bonds can affect the type and topology of the hybrid water containing associates within various [1,2,5]-thiadiazolo- [3,4-f]-[1,10]-phenanthroline (tdzp) transition metal complexes. Further the reversible dehydration and rehydration process in 2 was monitored by observing the changes in intensity of the infrared band corresponding to water in the FT-IR spectra of parent, dehydrated, and rehydrated samples. The water molecules from the crystal lattice were removed by heating the sample at 230 1C for 2 h. The comparative IR spectra of the parent crystalline solid of 2, dehydrated solid and rehydrated solid are given in Fig. S9, ESI.† The IR spectrum of parent 2 shows a broad band centred at around 3380 cm1 assigned to the O–H stretching frequency of the water cluster (Fig. S9, ESI†). The intensity of this band decreases significantly upon heating the parent sample at 230 1C for 2 h, suggesting the escape of water molecules. The exposing of the dehydrated sample of 2 to moisture overnight showed the reappearance of the band at 3382 cm1 . This result strongly suggests that dehydrated 2 is reversible in the solid state with reabsorption of the water molecule.

Photophysical properties

ISSN PRINT 2319 1775 Online 2320 7876

 Journal Volume 10, Iss 09, 2021

The absorption and emission spectra of complexes 1–3 are given in Fig. 4, and photophysical properties of complexes 1–3 in different solvents are summarized in Table 3. The absorption spectra of complexes 1–3 (Fig. 4) are dominated by high-energy bands between 240 to 340 nm which are related to the p - p* transitions of the aromatic nitrogen donor ligands.43,58,59 The band around 450 nm for complexes 1–3 is assigned as the MLCT Ru (dp) - ligand (p*) transitions typical of polypyridyl ruthenium(II) complexes.

The emission spectra of complexes 1–3 recorded in various solvents by excitation of the MLCT band at room temperature shows a characteristic broad emission peak at around 550– 750 nm (Fig. 4). The emission maxima, relative quantum yield in different solvents are given in Table 3. All complexes show solvent dependent properties and are highly luminescent. The emission quantum yield of complexes 1–3 in methanol and DMF is higher than that of [Ru(bpy)3] 2+.

DNA interaction studies

Before carringout DNA binding studies, the stability of complexes in water was checked by comparing the UV-Visible spectra of complexes recorded immediatly after dissolving in water and after 8th day of dissolving (Fig. S10, ESI†). The spectra show no obvious changes confirming the stability of these complexes in water.

Absorption titration

Electronic absorption spectroscopy is one of the most widely used techniques for exploring the interaction of metal complexes with DNA.21,31–36 Strong interaction of complex with DNA through

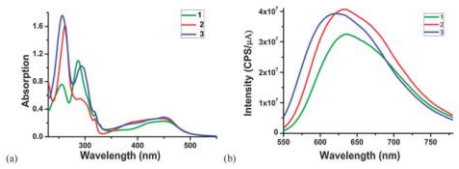

Fig. 4 Absorption (left) and emission (right) spectra of 1–3 in methanol (20 mM).

Table 3 UV/Vis and emission data for complexes 1–3

	Absorbance λ_{max} (nm)/ε (M^{-1} cm^{-1})		Emission					
	Methanol		Methanol		DMF		Water	
Complex[a]	Ligand transitions	MLCT	λ_{em}/nm	ϕ_{em}[d]	λ_{em}/nm	ϕ_{em}[d]	λ_{em}/nm	ϕ_{em}[d]
1	256/38 100 286/55 800 319/16 300	450/11 300	635	0.052	643	0.091	637	0.014
2	262/81 100 292/27 800 319/13 100	448/13 000	629	0.058	646	0.102	636	0.031
3	256/88 300 294/51 400 318/18 500	452/14 200	622	0.052	637	0.094	637	0.043
$[Ru(bpy)_3]^{2+}$[b]	—		630	0.045	629	0.063	630	0.042

[a] [Ru] = 20 (±0.2) μM. [b] Data taken from ref. 60. [c] Emission maxima. [d] ϕ = emission quantum yield, error limit: λ_{max} = ±2 nm, λ_{em} = ±2 nm, ϕ = ±5%.

intercalation leads to hypochromism and a red shift, due to the interaction between the aromatic chromophore of the complex and the base pairs of the DNA.30,61 The amount of hypochromism and red shift depends on the strength of the interaction of the complex with DNA.30–34,61 Changes in absorption spectra of complexes 1–3 with increasing concentration of DNA are shown in Fig. 5 and Fig. S11 (ESI†). The percentage of hypochromism and red shift for complexes 1–3 in the presence of CT-DNA are given in Table 4. The intrinsic binding constant of complexes 1–3 with CT-DNA is calculated using eqn (2) by observing the changes in the MLCT band with increasing concentration of DNA (Fig. 5 and Fig. S11, ESI†). The binding constants are 7.6 103 , 1.05 104 and 1.2 104 M1 for complexes 1–3 respectively. Binding constants for complexes are comparable to that of known DNA intercalators such as 3.9 105 M1 for [Ru(bpy)2(dcdpq)]2+ (dcdpq = dicyano-dipyrido[3,2-d:20 ,30 -f]quinoxaline),62 4.7 104 M1 for [Ru(bpy)2(dpq)]2+, 62 6.3 104 M1 for [Ru(bpy)2- (dpt)]2+ (dpt = 3-(pyrasin-yl)-as-triazino[5,6-f]phenanthrene),

ISSN PRINT 2319 1775 Online 2320 7876

 Journal Volume 10, Iss 09, 2021

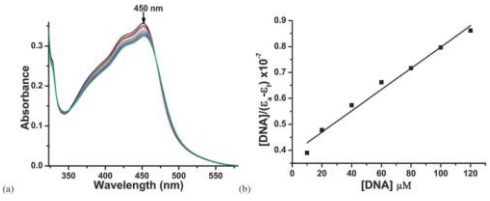

Fig. 5 (a) Changes in the electronic absorption spectra of complex 3 (20 mM), with increasing concentrations of CT-DNA (0–140 mM) (phosphate buffer, pH 7.2), (b) fitting of the absorbance data used to obtain the binding constant.

Table 4 Electronic absorption data upon addition of CT-DNA

Complex[a]	$\Delta\lambda_{max}$ (MLCT)	Hypochromism H[b] (%)			K_b (M^{-1})	Ref.
1	2	4.7 (448)	5.3 (286)	6.8 (256)	7.6×10^3	Present work
2	2	6.8 (450)	10.2 (292)	8.3 (260)	1.05×10^4	Present work
3	4	9.1 (452)	11.8 (294)	13.5 (256)	1.2×10^4	Present work
$[Ru(bpy)_2(dcdpq)]^{2+}$	2	20.0 (450)	—	—	3.9×10^5	62
$[Ru(bpy)_2(dpq)]^{2+}$	5	14.0 (453)	—	—	4.7×10^4	62
$[Ru(bpy)_2(dpz)]^{2+}$	5	18.1 (474)	—	—	6.3×10^4	63
$[Ru(bpy)_2(aip)]^{2+}$	—	—	23.0 (367)	43.0 (253)	4.9×10^4	64

[a] Ru = 20 μM ± 0.5 μM. [b] H% = 100 $(A_{free} - A_{bound})/A_{free}$ in phosphate buffer (pH = 7.2) where, A = absorbance, error limit: λ_{max} = ±2 nm, H (%) = ±5%; K_b (M^{-1}) = ±5%.

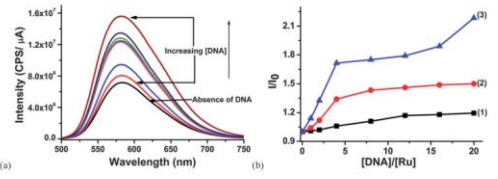

Fig. 6 Emission spectra of complexes (a) 3 (10 mM) in phosphate buffer, pH 7.2, at 298 K with increasing [CT-DNA]/[Ru] ratio 0–20; [complex] = 10 mM, [DNA] = 0–200 mM, (b) plot of relative integrated emission intensity versus [CT-DNA]/[Ru] for the complexes 4.9 ——————— 0.3 104 M1 for [Ru(bpy)2(aip)]2+ (aip = 2-(9-anthryl)-1Himidazo[4,5-f][1,10]phenanthroline).64 The spectral characteristic as well as Kb value suggests that the complexes 2 and 3 bind to DNA by the partial intercalative mode involving stacking interaction between the aromatic chromophore and base pairs of the DNA.

Emission titration

The investigation of changes in luminescence properties of ruthenium complexes in the presence of DNA provides useful information about the type of DNA binding modes.43,65 Changes in emission spectra of complexes (10 mM) in phosphate buffer (pH 7.2) with increasing concentrations of DNA is shown in Fig. 6 and Fig. S12 (ESI†). Complex 1 exhibits very weak enhancement in luminescence intensity after adding CT-DNA indicating weak binding of the complex with DNA by electrostatic interaction. But complexes 2 and 3 show larger enhancement in luminescence intensity indicating strong binding of complexes with DNA either by groove or partial intercalation mode. These results are consistent with that of absorption titration experiments. The increase in luminescence intensity is due to two reasons: firstly, the hydrophobic environment inside the DNA helix reduces the accessibility of water molecules to the complex, and secondly, the complex mobility is restricted at the binding site and so the vibrational mode of relaxation decreases.

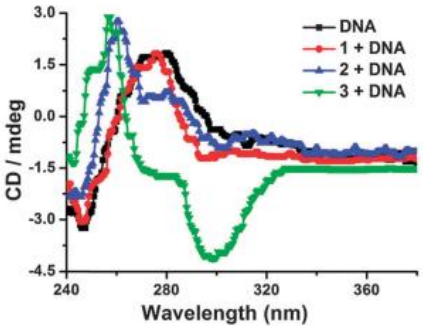

Fig. 7 CD spectra of CT-DNA in the presence and absence of complexes 1–3, in phosphate buffer (pH 7.2), [DNA]/[complex] = 4, [DNA] = 200 mM.

Circular dichroism spectral analysis

CD spectral analysis was used to monitor the conformational changes in DNA as a result of interaction with complexes with DNA.66,67 In CD spectrum of CT-DNA a positive band at 280 nm is assigned to the base pair stacking and band at 245 nm due to the right handed helicity characteristic of B-DNA.68 The CD spectrum of CT-DNA was sensitive to its conformational changes. The absorption and emission titration experiments show interaction of these complexes with DNA, and to further

ISSN PRINT 2319 1775 Online 2320 7876

 Journal Volume 10, Iss 09, 2021

confirm these interactions, circular dichroism (CD) spectra of DNA was recorded in the presence and absence of complexes 1–3. As shown in Fig. 7 in the presence of complex 1 small change in the CD spectrum of DNA was observed due to weak electrostatic interaction of the complex with DNA. In the case of complex 2 increase in the intensity of the positive band at 270 nm along with a blue shift of 18 nm was observed, which may be due to the groove or partial intercalation of complex 2 with DNA (Fig. 7). In presence of complex 3 larger changes in the CD spectrum of DNA was observed, the positive band at 270 nm is blue shifted by 22 nm and large enhancement of negative band intensity at 298 nm (Fig. 7) demonstrating the intercalative mode of binding with DNA

Electrophoretic mobility shift assay

In order to assess any damage of the DNA as a result of binding of these complexes, agarose gel electrophoresis has been performed with a circular form of plasmid pBR322 DNA. DNA cleavage ability of complexes 1–3 at low concentrations is shown in Fig. 8. Upon incubation of complexes 1–3 with plasmid pBR322 DNA under dark experimental conditions the conversion of super coiled DNA (Form I) into open circular DNA (Form II) was observed, but in the case of complex 3 conversion of supercoiled DNA into open circular as well as linear DNA was observed. At higher complex concentration and incubation time smearing of DNA bands was observed. The higher cleavage activity of complex 3 compared to complexes 1 and 2 is due to its higher DNA binding strength.

Cellular uptake and cytotoxicity studies

The cellular localization of complexes is monitored by fluorescence microscopy. Complexes are highly luminescent upon excitation at

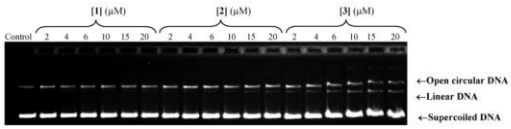

Fig. 8 Agarose (1%) gel electrophoresis of pBR 322 DNA under dark experimental conditions, [complex] = 2–20 mM, [DNA] = 200 ng, incubation time = 15 min, at 37 1C. TBE buffer, pH 8.2.

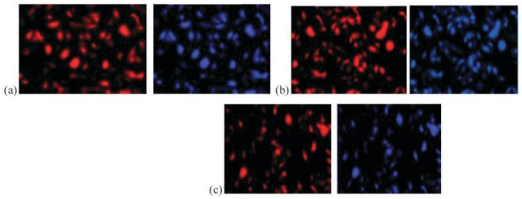

Fig. 9 Fluorescence microscopy images of HeLa cells incubated (48 h) with 15 mM of complexes and co-staining with DNA specific stain DAPI (a) cells incubated with complex 1 (left), DAPI co-staining (right); (b) cells incubated with complex 2 (left), DAPI co-staining (right); (c) cells incubated with complex 3 (left), DAPI co-staining (right).

the MLCT band and clearly visible within the cell after 24 h incubation (Fig. 9). To confirm the accumulation of the ruthenium complexes within the cell, a co-staining experiment with the DNAspecific dye DAPI (DAPI = 40 ,6-diamidino-2-phenylindole) was performed and strong co-localization of two emission signals was observed (Fig. 9), confirming nuclear staining by the complexes. The fluorescence microscopy images of cells clearly show that complexes 1–3 have staining patterns closely resembling to the standard DNA staining dye DAPI.

The in vitro cytotoxicity of complexes 1–3 against a HeLa (cervical) cancer cell line has been tested by MTT [3-(4,5-dimethylthiazol-2-yl)-2,5-

ISSN PRINT 2319 1775 Online 2320 7876

 Journal Volume 10, Iss 09, 2021

diphenyltetrazolium bromide] assay. These complexes exhibit significant cytotoxicity in a concentration dependent manner (Fig. 10). The percent cell viability of HeLa cell lines in the presence of complex 1–3 was measured in the concentration range of 1 mM to 50 mM, the compounds tested were found to be active at lower concentrations. Complexes 1–3 exhibits significant cytotoxicity against the HeLa cell line by inducing apoptosis and can be viewed as potential candidates for antitumor therapy. The IC50 values against HeLa cell line are 28 ——— 0.12, 21 ——— 0.08 and 19 ——— 0.08 mM for complex 1, 2 and 3 respectively. We think that anticancer activity of complexes 1–3 may not be only due to partial intercalation or groove binding, but also due to the specific chemical structure and the nature of the ligands used.

Conclusion

In summary, we have synthesized and characterized a series of mononuclear ruthenium(II) polypyridyl complexes 1–3. The molecular structure of complex 2 was confirmed by single crystal X-ray structure determination. We have crystallographically characterized the polymeric cyclic hybrid chloride–water cluster {[(H2O)10(Cl)2] 2}n encapsulated in complex 2. This water–chloride cluster has been trapped by a cationic ruthenium(II) polypyridyl cation, which is stabilized by strong hydrogen bonding interactions between the cationic unit and chloride anions–water molecules. All complexes show solvent dependent photophysical properties. All complexes interact with DNA and the order of binding of the complexes to DNA is 3 4 2 4 1 reflecting that the increase in planarity of ligands plays important role in DNA binding. Fluorescence microscopy studies reveal the nuclear staining by complexes and apoptosis mode of cell death. Notably, 1–3 exhibit potent

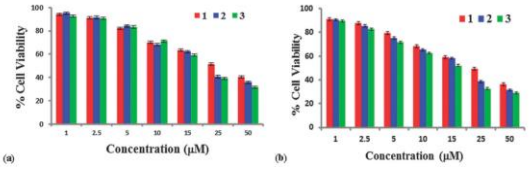

Fig. 10 Concentration dependent cytotoxicity of complexes 1–3 against a HeLa cell line evaluated by MTT assay, (a) after 48 h, (b) after 72 h. Results are mean values of three biological replicates and that in each biological replicate there were four technical replicates.

antiproliferative activities against a panel of human cancer cell lines. Given these properties, analogues of these complexes could be developed as novel agents as probes for the nucleic acid structure.

Experimental

Chemicals

All chemicals and solvents were purchased commercially and were used as received. RuCl33H2O was purchased from S. D. Fine chemicals, Mumbai (India), and calf thymus DNA was purchased from SRL, Kolkata (India), and used as received. pBR 322 DNA was purchased from Chromus Biotech Pvt. Ltd (India).

Synthesis

The ligands dipyrido[3,2-d:20 ,30 -f]quinoxaline (dpq),70,71 [1,2,5]-thiadiazolo-[3,4-f]-[1,10]-phenanthroline (tdzp)37,38 were synthesized according to the reported literature procedures. **[Ru(bpy)2(tdzp)]Cl23.5H2O (1).** The precursor complex cis-[Ru(bpy)2Cl2]2H2O (192 mg, 0.369 mM) and tdzp (90 mg, 0.369 mM) were dissolved in methanol–water solvent (1: 1, 50 mL) and the reaction mixture was

ISSN PRINT 2319 1775 Online 2320 7876

 Journal Volume 10, Iss 09, 2021

heated to reflux for 10 h. During this period the color of the solution changed from dark purple to red. The solution was filtered hot and was cooled to room temperature. The solvent was evaporated to obtain a red solid. The product obtained was purified by column chromatography (activated neutral alumina; acetone–methanol, 6: 4). The orange-red fraction was collected and evaporated to get the orange-red pure product. Yield: 185 mg (64.1%). 1 H NMR (DMSO-d6, 400 MHz, 25 1C): d (ppm) = 9.17 (dd, 2H), 8.96 (t, 4H), 8.27 (m, 4H), 8.15 (m, 2H), 7.99 (q, 2H), 7.81 (d, 2H), 7.74 (d, 2H), 7.61 (m, 2H), 7.40 (m, 2H). 13C NMR (DMSO-d6, 125 MHz, 25 1C): d (ppm) = 124.88, 125.02, 128.24, 128.25, 128.31, 130.0, 134.38, 138.48, 138.59, 140.52, 150.51, 151.91, 152.44, 154.51, 156.97, 157.26. IR (KBr, cm1): 3391 (H2O), 3018 (CH), 1632, 1604, 1467, 1440, 1407 (CQN, CQC). ESI-MS (m/z, positive mode): 326 (B100) ([M–2Cl]2+), 686.7 (B10%) ([M–Cl]+). Anal. calcd for C32H22N8Cl2SRu3.5H2O: C, 48.92; H, 3.72; N, 14.26; found: C, 48.71; H, 3.83; N, 14.01.

[Ru(phen)2(tdzp)]Cl26.5H2O (2). The synthesis and purification of complex 2 was similar to that of 1 using cis-[Ru(phen)2Cl2]2H2O (197 mg, 0.345 mM) and tdzp (80 mg, 0.345 mM). Yield: 235 mg (76.8%). 1 H NMR (DMSO-d6, 400 MHz, 25 1C): d (ppm) = 9.14 (dd, 2H), 8.82 (m, 4H), 8.43 (q, 4H), 8.25 (dd, 2H), 8.16 (dd, 2H), 8.05 (dd, 2H), 7.81 (m, 6H). 13C NMR (DMSO-d6, 125 MHz, 25 1C): d (ppm) = 125.36, 126.31, 126.42, 127.78, 128.11, 128.15, 130.51, 130.53, 133.17, 137.08, 147.08, 147.11,150.74, 151.33, 152.68, 153.39, 153.67. IR (KBr pellet, cm1): 3380 (H2O), 3018 (CH), 1621, 1604, 1430, 1402 (CQN, CQC). ESI-MS: (m/z, (%) positive mode): 350 (B100%) ([M–2Cl]2+), 734.7 (B7%) ([M–Cl]+). Anal. calcd for C36H22N8Cl2SRu6.5H2O: C, 48.71; H, 3.97; N, 12.62; found: C, 48.47; H, 3.79; N, 12.38.

[Ru(dpq)2(tdzp)]Cl22H2O (3). The synthesis and purification of complex 3 was similar to that of 1 using cis-[Ru(dpq)2Cl2] 2H2O (120 mg, 0.188 mM) and tdzp (45 mg, 0.188 mM). Yield: 112 mg (69.1%). 1 H NMR (DMSO-d6, 400 MHz, 25 1C): d (ppm) = 9.55 (m, 4H), 9.39 (s, 4H), 9.17 (d, 2H), 8.36 (m, 2H), 8.32 (d, 2H), 8.28 (d, 2H), 7.93 (m, 6H). 13C NMR (DMSO-d6, 125 MHz, 25 1C): d (ppm) = 160.13, 162.50, 162.99, 165.10, 165.49, 167.20, 170.81, 170.97, 171.09, 177.21, 184.49, 184.64, 186.85, 186.90, 188.30, 189.05, 189.55, 191.88, 192.13, 192.25. IR (KBr pellet, cm1): 3375 (H2O), 3021 (CH), 1627, 1604, 1479, 1457, 1402, 1391 (CQN, CQC). ESI-MS: (m/z, (%) positive mode): 402.1 (B100%) ([M–2Cl]2+), 838.7 (B7%) ([M–Cl]+). Anal. calcd for C40H22N12Cl2SRu2H2O: C, 52.75; H, 2.88; N, 18.46; found: C, 52.53; H, 2.73; N, 18.29.

Methods and instrumentation

1 H NMR spectra of the ligand and complexes were recorded on a Brucker 400 MHz spectrometer with DMSO (d6) as a solvent at room temperature and all chemical shifts are given relative to TMS. The IR spectra of complexes 1–3 dispersed in KBr were recorded on a Jasco 5300 FT/IR infrared spectrometer. Microanalysis (C, H, and N) were performed using a Thermo Quest microanalysis instrument capable of carrying out C, H, N (carbon, hydrogen, nitrogen) analysis. The electrospray mass spectra were recorded on a MICROMASS QUATTRO II triple quadrupole mass spectrometer using methanol as solvent. Absorption spectra of complexes were recorded on a Shimadzu UV-Vis-NIR

ISSN PRINT 2319 1775 Online 2320 7876

 Journal Volume 10, Iss 09, 2021

spectrophotometer. Emission spectra of complexes were carried out on a Fluoromax-4 spectrofluorimeter at room temperature. All absorption and emission Emission quantum yields (f) were calculated by integrating the area under the fluorescence curves and by using eqn (1).72measurements were carried out in the presence of oxygen.

$$\phi_{Sample} = \{OD_{Standard} \times A_{Sample}\}/\{OD_{Sample} \times A_{Standard}\} \times \phi_{Standard} \quad (1)$$

where, OD is optical density of the complex at the excitation wavelength (450 nm) and A is the area under the emission spectrum. The standard used for the quantum yield measurements was [Ru(bpy)3]Cl2. 60 Emission quantum yield was determined by using 20 mM solutions of complexes 1–3 and standard [Ru(bpy)3]Cl2 at room temperature in methanol, dimethyl formamide and water solvents.

X-ray crystallography

The unit cell parameters and the intensity data at 100 K for 2 were obtained on a Bruker SMART APEX CCD 1000 area detector, using graphite-monochromated Mo-Ka radiation (l = 0.71073 Å). The data was reduced using SAINTPLUS73 and a multi-scan absorption correction using SADABS74 was performed. The structure of 2 was solved by direct methods and refined on F2 by full-matrix least-squares procedures. The non-hydrogen atoms were refined using anisotropic thermal parameters. The hydrogen atoms were included in the structure factor calculations at idealised positions using a riding model. Structure solution and refinement were performed using the SHELXS9775 available in the WinGX package.76 The ORTEP,77 Platon78 and Mercury packages79 were used for molecular graphics. CCDC 1027779.

DNA binding studies

The concentration of CT-DNA was determined from its known extinction coefficient at 260 nm (6600 M1 cm1) in phosphate buffer solution. Solutions of calf thymus DNA gave a ratio of UV absorbance at 260 and 280 nm, A260/A280 of 1.8–1.9 signifying that the DNA was sufficiently free of protein. For absorption titration assays, the complex concentration (20 mM) was kept constant and DNA concentration was varied from 0–140 mM. After each addition of DNA to the metal complex, the resulting solution was mixed using a pipette 30 times and allowed to equilibrate at 25 1C for 15 minutes, after which absorption readings were noted. The data were then fit to eqn (2)80 to obtain intrinsic binding constant Kb.

$$[DNA]/[\varepsilon_a - \varepsilon_f] = [DNA]/[\varepsilon_b - \varepsilon_f] + 1/K_b[\varepsilon_b - \varepsilon_f] \quad (2)$$

where, [DNA] = concentration of DNA in base pairs, ea = extinction coefficient observed for the MLCT absorption band at the given DNA concentration, ef = the extinction coefficient of the complex in solution and eb = the extinction coefficient of the complex when fully bound to DNA. The plot of [DNA]/[ea ef] versus [DNA] gave a slope 1/[ea ef] and Y intercept is equal to 1/Kb[eb ef], respectively. The intrinsic binding constant Kb is the ratio of the slope to the intercept.80,81 For emission titration experiments increasing concentration of the DNA was added to a fixed concentration of complex. The concentration of complex used was 10 mM and [DNA]/[Ru] ratio was between 0–20. After the addition of DNA to the complex solution, the resulting solution was allowed to equilibrate for 15–20 minutes at room temperature. Then the emission spectra were recorded by exciting at metal to ligand charge-transfer band at 450 nm.

ISSN PRINT 2319 1775 Online 2320 7876

 Journal Volume 10, Iss 09, 2021

The excitation and emission slit widths were 5 nm each.

DNA cleavage studies

For the agarose (1%) gel electrophoresis experiments23,25 the super coiled pBR 322 DNA (200 ng in nucleotide) in TBE buffer (89 mM Tris-borate acid, 2 mM EDTA, pH 8.2) was reacted with the complexes 1–3 (2 mM to 20 mM) and the reaction mixture was incubated at 37 1C in dark for 30 minutes, after incubation the reaction was quenched by the addition of 2 mL gel loading dye (0.25% bromophenol blue, 0.25% xylene cyanol, 40% glycerol and 2 mM EDTA). The samples were subjected to electrophoresis at 60 V on 1% agarose gel in TBE (Tris-boric acid–EDTA) buffer (pH 8.2). The gel was stained with a 0.5 mg mL1 ethidium bromide and visualized by UV light and photographed for analysis using the Alpha Innotech Gel documentation system (AlphaImager 2200).

Cytotoxicity: cell viability assay

Cytotoxicity experiments were carried out as per our previous reports.23,25 The viable cells remaining after appropriate treatment of the complexes were determined by 3-(4,5-dimethylthiazol-2-yl)- 2,5-diphenyltetrazolium bromide (MTT; Sigma Chemical Co.) assay. The cells were placed (4000 cells per well per 0.2 mL DMEM medium) in 96-well microtiter plates and incubated overnight.

Then complexes 1–3 were added to three biological replicates (in each biological replicate there were four technical replicates). After incubation (48 and 72 h) MTT was added to each well at a final volume of 0.5 mg mL1 and the microplates were incubated at 37 1C for 3 h. Then supernatant was removed, the formazan salt resulting from the reduction of MTT was dissolved in dimethyl sulfoxide and the absorbance was recorded at 570 nm using an automatic plate reader (Thermo Corporation). The cell viability was extrapolated from optical density (OD) 570 nm values and expressed as percent survival.

Acknowledgements

S. S. Bhat acknowledges University Grants Commission, New Delhi, India, for providing Dr D. S. Kothari Postdoctoral grant (Award Letter No. 13-856/2013(BSR)). S. S. Bhat acknowledges Professor M. V. Rajasekharan for useful discussions and suggestions. Authors are also grateful to UGC Networking Resource Centre, School of Chemistry, and University of Hyderabad for providing the laboratory and instrumental facilities. We thank SAIF, CDRI-Lucknow, India, for providing ESI-MS data and elemental analysis data.

references

1 C. Metcalfe and J. A. Thomas, Chem. Soc. Rev., 2003, 32, 215–224.

2 A. E. Friedman, J. C. Chambron, J. P. Sauvage, N. J. Turro and J. K. Barton, J. Am. Chem. Soc., 1990, 112, 4960–4962.

3 S. Ramakrishnan, E. Suresh, A. Riyasdeen, M. A. Akbarsha and M. Palaniandavar, Dalton Trans., 2011, 40, 3524–3536.

4 M. R. Gill and J. A. Thomas, Chem. Soc. Rev., 2012, 41, 3179–3192.

5 Q. Zhao, C. Huang and F. Li, Chem. Soc. Rev., 2011, 40, 2508–2524.

6 G. Liao, X. Chen, J. Wu, C. Qian, H. Wang, L. Ji and H. Chao, Dalton Trans., 2014, 43, 7811–7819.

7 Z. Zhu, L. Xu, H. Li, X. Zhou, J. Qin and C. Yang, Chem. Commun., 2014, 50, 7060–7062.

ISSN PRINT 2319 1775 Online 2320 7876

 Journal Volume 10, Iss 09, 2021

8 C. Santini, M. Pellei, V. Gandin, M. Porchia, F. Tisato and C. Marzano, Chem. Rev., 2014, 114, 815–862.

9 M.-J. Li, T.-Y. Lan, X.-H. Cao, H.-H. Yang, Y. Shi, C. Yi and G.-N. Chen, Dalton Trans., 2014, 43, 2789–2798.

10 S. P. Dash, A. K. Panda, S. Pasayat, R. Dinda, A. Biswas, E. R. T. Tiekink, Y. P. Patil, M. Nethaji, W. Kaminsky, S. Mukhopadhyay and S. K. Bhutia, Dalton Trans., 2014, 43, 10139–10156.

11 X.-B. Fu, D.-D. Liu, Y. Lin, W. Hu, Z.-W. Mao and X.-Y. Le, Dalton Trans., 2014, 43, 8721–8737.

12 B. Pen˜a, A. David, C. Pavani, M. S. Baptista, J.-P. Pellois, C. Turro and K. R. Dunbar, Organometallics, 2014, 33, 1100–1103.

13 B. Elias and A. K.-D. Mesmaeker, Coord. Chem. Rev., 2006, 250, 1627–1641.

14 J. G. Vos and J. M. Kelly, Dalton Trans., 2006, 4869–4883.

15 N. J. Turro, J. K. Barton and A. T. Donald, Acc. Chem. Res., 1991, 24, 332–340.